Eddy kinetic energy and small-scale sea level height variability*

A. Kaplan
Lamont-Doherty Earth Observatory of Columbia University, Palisades, NY 10964

March 2003

Abstract

A mathematical connection is established between the ocean near-surface geostrophic kinetic energy and the small-scale variance of its surface height. The latter is defined as the spatial variance of sea surface height inside a given grid box and represents a basic statistical characteristic of the field, necessary for estimating its vulnerability to sampling error. The former is also computed from sea surface height fields and, being an important dynamical attribute of the ocean, is often used to describe its mesoscale variability, or eddy energy. Under the condition of isotropic distribution of mesoscale energy, simple formulas connecting the two are obtained for the long- and short-wave (compared to the grid scale) portions of the ocean power spectrum. Without these simplifying assumptions, a factor depending on the actual location-dependent two-dimensional wavenumber power spectrum enters the equation. Approximations based on the Stammer (1997) one-dimensional power spectrum estimates are developed. They are verified by application to the Ducet et al. (2000) gridded satellite altimetry fields.

Keywords: Sea level height, geostrophic kinetic energy, eddies, small-scale variability, wavenumber power spectrum, satellite altimetry.

1 Introduction

Oceanographers have long been interested in the global distribution of mesoscale variability in the ocean. With progress in satellite altimetry, techniques for estimating this pattern have been getting more elaborate, and the pattern estimates themselves more detailed. Early estimates of this pattern could be based on just a month of SEASAT data (Cheney et al. 1983), or a year of the Geosat mission (Fu et al. 1988), and mesoscale variability was expressed in terms of the temporal standard deviation of altimetric values from repeat tracks. In the Topex/Poseidon (T/P) period an explicit computation of the geostrophic kinetic energy (GKE) became the most common way to map the mesoscale variability. Stammer (1997) (hereafter S97) and Stammer and Wunsch (1999) used only along-track derivatives of altimetric values, under an assumption of isotropy of the turbulent eddy field. Later, when merging T/P and ERS-1,2 data allowed a fine gridding of global altimetry (0.25^o spatial and 10 day temporal resolution), Ducet et al. (2000) (hereafter DLTR) computed the

*submitted as note to *Journal of Physical Oceanography*

eddy GKE $\langle \mathcal{K} \rangle$ via both components of the geostrophic velocity. (Hereafter angle brackets denote long-term time averaging, unless some other type of average is explicitly indicated.)

A basic statistical characteristic of sea surface height field, its small-scale variance (SSV) $\langle \sigma^2 \rangle$ (Figure 1a), has a pattern which is very similar to that of the GKE $\langle \mathcal{K} \rangle$ (Figure 1b; cf. Plate 8 in DLTR). Naturally, the SSV depends on the spatial length below which the variability scale is considered "small". The values presented in Figure 1a are spatial variances inside $4^o \times 4^o$ gridboxes. SSV of climate fields is necessary for evaluating sampling error of its estimates (Leith 1973, Trenberth et al. 1992, Kaplan et al. 1997). Therefore, in addition to its contribution to the total sea surface height variability, the SSV plays an important role in estimating sampling error and error of gridding for various types of analyzed sea level height data sets (Le Traon et al. 1990, Kaplan et al. 2003).

The similarity between the patterns of Figures 1a and 1b can be clearly seen in a scatter plot (Figure 2a): values corresponding to each latitude group along parallel straight lines whose offsets from each other are mainly due to the dependence of the Coriolis parameter $f = 2\Omega \sin\theta$ on latitude θ ($\Omega = 2\pi/\text{day}$ is the earth rotation rate). Influence of the Coriolis parameter can be excluded by using $\mathcal{G}$, the squared gradient of sea surface height, instead of $\mathcal{K}$ (Figure 1c). Note that $\mathcal{G} = 2f^2\mathcal{K}/g^2$ (g is the acceleration of gravity) differs just by a constant factor from the equivalent slope variance $\mathcal{K}_{sl} = \mathcal{K}\sin^2\theta = g^2\mathcal{G}/8\Omega^2$ which is often used to exclude the equatorial singularity that is due to the vanishing Coriolis parameter (e.g. S97, Wunsch and Stammer 1999). Removal of the dependence on f results in even stronger resemblance with the pattern of the SSV. The scatter plot of Figure 2b shows that values of $\mathcal{G}$ at different latitudes are grouped much closer to each other compared to the values of $\mathcal{K}$ in Figure 2a, even though some latitudinal dependence of the ratio $\langle \sigma^2 \rangle / \langle \mathcal{G} \rangle$ remains.

The spatial similarity between the equivalent slope variance and small-scale variance was noted before (e.g. S97). This similarity (between the $\mathcal{K}$, $\mathcal{K}_{sl}$, or $\mathcal{G}$ on one hand and the SSV $\langle \sigma^2 \rangle$ on the other hand) is expected since both variable types characterize the magnitude of sea level height differences between nearby locations. Yet, since σ^2 is an important statistical characteristic of a continuous sea level height field, crucial for evaluating its sampling error, and $\mathcal{K}$ is a basic dynamical characteristic of the ocean, widely used for describing its mesoscale variability, it is important to substantiate the formal reason for their similarity, and express this similarity mathematically, in a quantitative and verifiable way. This note provides such a derivation, makes useful approximations for the factors involved, and verifies the results.

Necessary definitions are given in Section 2. In Section 3 simple formulas are derived for asymptotic cases when the isotropically turbulent ocean is dominated by either very long or very short waves (compared to the chosen grid size). If these simplifying assumptions are not applicable, the connection between the SSV and GKE involves a coefficient which depends on the actual location-dependent two-dimensional wavenumber power spectrum of the ocean sea surface height (Section 4). Approximations based on the S97 one-dimensional power spectrum estimates are developed. They are verified by application to the DLTR data set of satellite altimetry fields in Section 5. Discussion and conclusions are presented in Section 6.

2 Data and definitions

Kinetic energy and related terms. The geostrophic kinetic energy is

$$\mathcal{K} = \mathcal{K}_u + \mathcal{K}_v = \frac{u_g^2}{2} + \frac{v_g^2}{2}$$

where geostrophic velocities

$$u_g = -\frac{g}{f}\frac{\partial s}{\partial y} \qquad v_g = \frac{g}{f}\frac{\partial s}{\partial x}$$

are estimated from derivatives of sea surface height $s(x, y)$.

Define

$$\mathcal{G} = |\vec{\nabla} s|^2 = \mathcal{G}_x + \mathcal{G}_y = \left(\frac{\partial s}{\partial x}\right)^2 + \left(\frac{\partial s}{\partial y}\right)^2. \tag{1}$$

Obviously,

$$\mathcal{K} = \frac{g^2}{2f^2}\mathcal{G}; \qquad \mathcal{K}_u = \frac{g^2}{2f^2}\mathcal{G}_y; \qquad \mathcal{K}_v = \frac{g^2}{2f^2}\mathcal{G}_x. \tag{2}$$

Given a field $s(x, y)$ gridded with steps Δx and Δy, so that $x = m\Delta x$ and $y = n\Delta y$, and $s_{m,n} = s(m\Delta x, n\Delta y)$, gradient components can be estimated via a finite difference approximation. The first central difference will be used throughout this note:

$$\mathcal{G}_x = \left[\frac{s_{m+1,n} - s_{m-1,n}}{2\Delta x}\right]^2, \qquad \mathcal{G}_y = \left[\frac{s_{m,n+1} - s_{m,n-1}}{2\Delta y}\right]^2. \tag{3}$$

Small-scale variance (SSV). In practical calculations with gridded data, instead of a continuous distribution $s(x, y)$ inside the grid box $G = L_x{\times}L_y$ we only have values of s for $N = L_xL_y/\Delta x\Delta y$ smaller grid boxes contained inside G: $\{s_i,\ i{=}1, \cdots, N\}$. The true mean over the grid box has to be replaced by sample estimates

$$\overline{s} = \frac{1}{N}\sum_{i=1}^{N} s_i,$$

the true variance σ_G^2 is replaced by

$$\widehat{\sigma}_G^2(s) = \frac{1}{N-1}\sum_{i=1}^{N}(s_i - \overline{s})^2 = \frac{N}{N-1}\left(\overline{s^2} - \overline{s}^2\right) \tag{4}$$

to obtain an unbiased sample estimate of the noise variability inside the grid box G (e.g. Mardia et al. 1979).

Data and averaging. For practical computations in this note the DLTR analyses of satellite altimetry are used. Their spatial resolution $\Delta x{\times}\Delta y$ is 0.25^o in both zonal and meridional directions. Temporal resolution is 10 days. Given scales L_x and L_y, SSV values for the $L_x \times L_y$ grid boxes are computed by formula (4). Values of $\mathcal{K}$ and related terms are computed by formulas (1) and (2), and then averaged to the $L_x \times L_y$ grid boxes for which the SSV values are available. Finally, all computed values are then averaged for the period from October 1992 to August 2001 (except for the period from December 24, 1993 to March 24, 1995 when fields in the DLTR data set are missing due to the gap in the ERS-1 data) to obtain statistically stable estimates $\langle\mathcal{K}\rangle$, $\langle\mathcal{G}\rangle$, $\langle\sigma_G^2\rangle$, etc. Assuming all processes are ergodic, these temporal averages can be interpreted as statistical ensemble means, i.e. expected values.

3 Long- and short-wave approximations

General. Using the following identity for a sample $\{s_i, \quad i = 1, \cdots, N\}$

$$\sum_{i<j}(s_i - s_j)^2 = N\sum_i s_i^2 - \left(\sum_i s_i\right)^2,$$

the SSV estimate (4) can be rewritten as a half of the mean squared difference between individual observations:

$$\hat{\sigma}_G^2 = \frac{1}{N-1}\sum_i s_i^2 - \frac{1}{(N-1)N}\left(\sum_i s_i\right)^2 = \frac{1}{(N-1)N}\left(N\sum_i s_i^2 - \left(\sum_i s_i\right)^2\right) = \frac{1}{(N-1)N}\sum_{i<j}(s_i - s_j)^2 = \frac{1}{2N(N-1)}\sum_{i\neq j}(s_i - s_j)^2 = \frac{1}{2}\langle (s_i - s_j)^2\rangle_{i\neq j}. \quad (5)$$

For a sample comprised of all gridded values $s_{m,n}$ inside a spatial gridbox $L_x \times L_y$ of a sparser grid, the SSV estimate (4) can be written as

$$\hat{\sigma}^2_{L_x\times L_y} = \frac{1}{2}\langle (s_{m_1,n_1} - s_{m_2,n_2})^2\rangle_{(m_1,n_1)\neq(m_2,n_2)}. \quad (6)$$

Isotropy assumption. It is easy to see from (1) and (2), that the isotropy assumption for the GKE is equivalent to the statement that the expected square of the sea surface height partial derivative does not depend on the direction of differentiation $\vec{n}$:

$$\left\langle \left(\frac{\partial s}{\partial \vec{n}}\right)^2 \right\rangle = \langle \mathcal{G}_x\rangle = \langle \mathcal{G}_y\rangle = \langle \mathcal{G}\rangle/2. \quad (7)$$

Long-wave approximation. Suppose sea level height s values are available on a fine grid with steps Δx and Δy inside a gridbox $L_x \times L_y$ of a sparser grid. If the sea level field is dominated by the waves longer than L_x and L_y (long-wave approximation), then for any two gridpoints (m_1, n_1) and (m_2, n_2) inside the box the assumption (7) results in the following expression for the expected value

$$\left\langle \left[\frac{s_{m_1,n_1} - s_{m_2,n_2}}{\sqrt{(m_1-m_2)^2\Delta x^2 + (n_1-n_2)^2\Delta y^2}}\right]^2 \right\rangle = \frac{1}{2}\langle \mathcal{G}\rangle,$$

and therefore

$$\langle (s_{m_1,n_1} - s_{m_2,n_2})^2\rangle = \frac{1}{2}\langle \mathcal{G}\rangle[(m_1-m_2)^2\Delta x^2 + (n_1-n_2)^2\Delta y^2]. \quad (8)$$

(Hereafter $L_x = M\Delta x$ and $L_y = N\Delta y$, so that $m = 1\ldots M, \quad n = 1\ldots N$).

Inserting (8) into (6) obtain

$$\hat{\sigma}_G^2 = \frac{1}{2}\langle (s_{m_1,n_1} - s_{m_2,n_2})^2\rangle_{(m1,n_1)\neq(m_2,n_2)} = \frac{1}{4}\langle \mathcal{G}\rangle[\langle (m_1-m_2)^2\rangle_{m_1\neq m_2}\Delta x^2 + \langle (n_1-n_2)^2\rangle_{n_1\neq n_2}\Delta y^2].$$

Using (5) backwards obtain

$$\langle (m_1-m_2)^2\rangle_{m_1\neq m_2} = 2\sigma_m^2 = \frac{2}{M-1}\left(\sum_i i^2 - \frac{1}{M}\left(\sum_i i\right)^2\right) = \frac{2}{M-1}\left(\frac{M(M+1)(2M+1)}{6} - \frac{1}{M}\left(\frac{M(M+1)}{2}\right)^2\right) = \frac{M(M+1)}{6},$$

and a similar expression for $\langle (n_1-n_2)^2\rangle_{n_1\neq n_2}$. Therefore in the long-wave approximation

$$\hat{\sigma}_G^2 \approx \frac{L_x^2 + L_y^2}{24}\langle \mathcal{G}\rangle, \quad (9)$$

where Δx and Δy were neglected in comparison with L_x and L_y respectively (i.e. assume $M \gg 1,\ N \gg 1$).

Short-wave approximation. In this case

$$\langle (s_{m+1,n} - s_{m,n})^2 \rangle = \frac{1}{2}\langle \mathcal{G} \rangle \Delta x^2, \qquad \langle (s_{m,n+1} - s_{m,n})^2 \rangle = \frac{1}{2}\langle \mathcal{G} \rangle \Delta y^2$$

holds, but the differences between neighboring points are uncorrelated with each other. Thus

$$\langle (s_{m_1,n_1} - s_{m_2,n_2})^2 \rangle = \frac{1}{2}\langle \mathcal{G} \rangle [|m_1 - m_2|\Delta x^2 + |n_1 - n_2|\Delta y^2] \tag{10}$$

(variance grows as in a random walk process).

Insert (10) into (6) and use the identity

$$\langle |m_1 - m_2| \rangle_{m_1 \neq m_2} = \frac{2}{M(M-1)} \sum_{1 \leq m_1 < m_2 \leq M} |m_1 - m_2| = \frac{2}{M(M-1)} \sum_{m=0}^{M} m(M-m) = \frac{2}{M(M-1)} \left[\frac{M^2(M+1)}{2} - \frac{M(M+1)(2M+1)}{6} \right] = \frac{M+1}{3}$$

to obtain

$$\hat{\sigma}_G^2 \approx \frac{1}{12}\langle \mathcal{G} \rangle (L_x \Delta x + L_y \Delta y) \tag{11}$$

with the same assumptions as above.

Intermediate wavenumbers. Formulas (9) and (11) can be written as

$$\hat{\sigma}_G^2 = \alpha_G \frac{L_x^2 + L_y^2}{12}\langle \mathcal{G} \rangle, \tag{12}$$

where a coefficient $\alpha_G \approx 0.5$ in the long-wave case and for short waves $\alpha_G = (L_x \Delta x + L_y \Delta y)/(L_x^2 + L_y^2) \leq \max(\Delta x/L_y, \Delta x/L_y) = 1/\min(M, N)$ is small when both N and M are large. This suggests that for the isotropically turbulent ocean formula (9) gives an upper-bound for the ratio $\alpha_G = 12\hat{\sigma}_G^2/[(L_x^2 + L_y^2)\langle \mathcal{G} \rangle]$. The value of α_G can reach 0.5 for the isotropic ocean dominated by waves much longer than L_x and L_y, but decreases when the waves become shorter. It tends to zero when decorrelation scales of a sea surface height field become small compared to the grid box dimensions . In order to make these statements more precise, sea surface height fields with general power spectrum need to be considered.

4 General power spectrum

Individual waves. Suppose a waveform of a unit amplitude with wavenumbers k_x and k_y

$$s(x, y) = e^{i2\pi(k_x x + k_y y)}$$

propagates through a space bin of dimensions L_x and L_y. It is easy to calculate the following statistics (notation as in section 2):

$$\mathcal{G} = \frac{1}{L_x L_y} \int_0^{L_y} \int_0^{L_x} 4\pi^2 (k_x^2 + k_y^2) \left| e^{i2\pi(k_x x + k_y y)} \right|^2 dxdy = 4\pi^2 (k_x^2 + k_y^2), \tag{13}$$

and $\mathcal{G}_x = 4\pi^2 k_x^2, \qquad \mathcal{G}_y = 4\pi^2 k_y^2$. Also

$$\overline{s} = \frac{1}{L_x L_y} \int_0^{L_y} \int_0^{L_x} e^{i2\pi(k_x x + k_y y)} dxdy = -\frac{(e^{i2\pi k L_x} - 1)(e^{i2\pi k L_y} - 1)}{4\pi^2 k_x k_y L_x L_y},$$

$$\sigma^2_{L_x\times L_y} = \overline{|s|^2} - |\overline{s}|^2 = 1 - \left|\frac{(e^{i2\pi kL_x}-1)(e^{i2\pi kL_y}-1)}{4\pi^2 k_x k_y L_x L_y}\right|^2 =$$
$$= 1 - \frac{4(1-\cos 2\pi k_x L_x)(1-\cos 2\pi k_y L_y)}{(4\pi^2 k_x k_y L_x L_y)^2}. \qquad (14)$$

Introducing

$$\mathcal{C}(\lambda) = \frac{2(1-\cos 2\pi\lambda)}{(2\pi\lambda)^2} = \left(\frac{\sin\pi\lambda}{\pi\lambda}\right)^2, \qquad (15)$$

can rewrite (14) as

$$\sigma^2_{L_x\times L_y} = 1 - \mathcal{C}(\lambda_x)\mathcal{C}(\lambda_y), \qquad (16)$$

where $\lambda_x = k_x L_x$ and $\lambda_y = k_y L_y$ are dimensionless parameters. Note that $\mathcal{C}(0) = 1$ and $0 \le \mathcal{C}(\lambda) \le 1$ for all λ, since $|\sin x/x| \le 1$.

If averaging is done only in x (or y) direction, then from (16) the formulas for one-dimensional variance:

$$\sigma^2_{L_x} = 1 - \mathcal{C}(\lambda_x), \qquad \sigma^2_{L_y} = 1 - \mathcal{C}(\lambda_y). \qquad (17)$$

Obviously

$$0 \le \sigma^2_{L_x} \le 1, \qquad 0 \le \sigma^2_{L_y} \le 1 \qquad (18)$$

It easily follows from (16) and (17), that

$$\sigma^2_{L_x\times L_y} = \sigma^2_{L_x} + \sigma^2_{L_y} - \sigma^2_{L_x}\sigma^2_{L_y}. \qquad (19)$$

For a single waveform the parameter α is

$$\alpha_{L_x\times L_y}(k_x,k_y) = \frac{12\sigma^2_{L_x\times L_y}}{(L_x^2+L_y^2)\mathcal{G}} = \varrho(\lambda_x,\lambda_y)\frac{1+\ell\kappa}{2}. \qquad (20)$$

Here

$$\varrho(\lambda_x,\lambda_y) = \frac{3(1-\mathcal{C}(\lambda_x)\mathcal{C}(\lambda_y))}{\pi^2(\lambda_x^2+\lambda_y^2)}, \qquad (21)$$

while ℓ and κ measure the "anisotropy" of the gridbox and of the waveform respectively:

$$\ell = \frac{L_x^2 - L_y^2}{L_x^2 + L_y^2}, \qquad \kappa = \frac{k_x^2 - k_y^2}{k_x^2 + k_y^2}. \qquad (22)$$

Both ℓ and κ take values from -1 to 1, reaching these extremes when either of their arguments is 0, and vanishing when the arguments are equal. Therefore, the factor $(1+\ell\kappa)/2$ in (20) is close to 1/2 if either ℓ or κ is small, but can reach 1 (or 0), if they approach their extremes of the same (or opposite) sign. The function $\varrho(\lambda_x,\lambda_y) \to 0$ when $\lambda_x^2+\lambda_y^2 \to \infty$. When $\lambda_x^2+\lambda_y^2 \to 0$, $\varrho \to 1$, since for small λ_x and λ_y the approximation $\mathcal{C}(\lambda) = 1 - \pi^2\lambda^2/3 + o(\lambda^3)$ can be used, and (21) gives

$$\varrho(\lambda_x,\lambda_y) \approx \frac{3\pi^2(\lambda_x^2+\lambda_y^2)/3}{\pi^2(\lambda_x^2+\lambda_y^2)} = 1.$$

Therefore $0 \le \alpha_{L_x\times L_y}(k_x,k_y) \le 1$. Note that in the long-wave limit ($\lambda_x \ll 1,\ \lambda_y \ll 1$), for the waveforms with $\kappa \approx 0$ formula (20) gives $\alpha = 1/2$, in agreement with (9).

Spectral distribution. Since the waveforms with different wavenumbers do not give "mixed" contributions in the quadratic products which appear in (13) and (14), the ratio $\alpha^{\mathcal{P}}_{L_x\times L_y}$ can be computed as

$$\alpha^{\mathcal{P}}_{L_x\times L_y} = \frac{12}{L_x^2+L_y^2}\frac{\int_{-\infty}^{\infty}\int_{-\infty}^{\infty}\sigma^2_{L_x\times L_y}\mathcal{P}dk_xdk_y}{\int_{-\infty}^{\infty}\int_{-\infty}^{\infty}\mathcal{G}\mathcal{P}dk_xdk_y} = \frac{\int_{-\infty}^{\infty}\int_{-\infty}^{\infty}\alpha_{L_x\times L_y}(k_x,k_y)\mathcal{G}\mathcal{P}dk_xdk_y}{\int_{-\infty}^{\infty}\int_{-\infty}^{\infty}\mathcal{G}\mathcal{P}dk_xdk_y} \tag{23}$$

for the ocean where the power spectrum of sea surface height $\mathcal{P}(k_x,k_y)$ is known. Formulas (13), (20), (21), and (22) can be used for direct computation of integrals in (23). Note that since $\mathcal{G}\mathcal{P}$ is positive, by the mean value theorem (e.g. Buck, 1965)

$$\alpha^{\mathcal{P}}_{L_x\times L_y} = \alpha_{L_x\times L_y}(k_x^*,k_y^*),$$

for certain k_x^* and k_y^*. Therefore $\alpha^{\mathcal{P}}_{L_x\times L_y}$ has to lie between 0 and 1 as well.

The direct computation by formula (23) requires knowledge of the true two-dimensional wavenumber spectrum $\mathcal{P}(k_x,k_y)$ for the global sea surface height fields, which is not presently available. However, in his analyses of T/P data, S97 found that a single parameterization of the one-dimensional wavenumber power spectrum is consistent with along-track sea surface height variability in all locations outside of the tropics. The tropical variability spectrum was approximated by a simpler, albeit less precise relationship. With the assumption of isotropy the along-track spectrum can be transformed into a radially-symmetric two-dimensional spectrum (S97, Le Traon et al. 1990, Fu et al. 1983). However, the use of this assumption for realistic ocean fields is at odds with significant differences between $\langle\mathcal{K}_u\rangle$ and $\langle\mathcal{K}_v\rangle$ found by DLTR in most locations (cf. their Plate 9). Therefore, it is assumed here that shapes of one-dimensional spectra in both zonal and meridional directions can be approximated by the S97 along-track spectral form, while the total amount of energy depends on direction. In other words, the estimates of one-dimensional wavenumber spectra in zonal and meridional directions

$$\begin{aligned}\mathcal{P}_x(k_x) &\sim \int\mathcal{P}(k_x,k_y)dk_y\\ \mathcal{P}_y(k_y) &\sim \int\mathcal{P}(k_x,k_y)dk_x\end{aligned} \tag{24}$$

are assumed to be consistent with the along-track spectral shape derived by S97. In practice, these integrals will be a sum over all available wavenumbers.

It is easy to check that the formula (20) for α works for one-dimensional averages as well, if both the wavenumber and gridsize of an "unused" dimension are put to zero (resulting in $\ell\kappa = 1$):

$$\begin{aligned}\alpha_{L_x}(k_x) &= \frac{12}{L_x^2}\frac{\sigma^2_{L_x}}{\mathcal{G}_x} = \frac{3(1-\mathcal{C}(\lambda_x))}{\pi^2k_x^2L_x^2} = \alpha_{L_x\times 0}(k_x,0),\\ \alpha_{L_y}(k_y) &= \frac{12}{L_y^2}\frac{\sigma^2_{L_y}}{\mathcal{G}_y} = \frac{3(1-\mathcal{C}(\lambda_y))}{\pi^2k_y^2L_y^2} = \alpha_{0\times L_y}(0,k_y).\end{aligned} \tag{25}$$

This makes it possible to compute α for one-dimensional averages by estimating factors

$$\alpha^{\mathcal{P}}_{L_x} = \frac{\int\alpha_{L_x}(k_x)k_x^2\mathcal{P}_x(k_x)dk_x}{\int k_x^2\mathcal{P}_x(k_x)dk_x}, \qquad \alpha^{\mathcal{P}}_{L_y} = \frac{\int\alpha_{L_y}(k_y)k_y^2\mathcal{P}_y(k_y)dk_y}{\int k_y^2\mathcal{P}_y(k_y)dk_y}. \tag{26}$$

Estimates for two-dimensional averages. Multiply both sides of (19) by $\mathcal{P}$ and integrate over k_x and k_y, to obtain that for a certain k_x^*

$$\sigma^{2\,\mathcal{P}}_{L_x\times L_y} = \sigma^{2\,\mathcal{P}}_{L_x} + \int_{-\infty}^{\infty}\int_{-\infty}^{\infty}(1-\sigma^2_{L_x})\sigma^2_{L_y}\mathcal{P}dk_xdk_y = \sigma^{2\,\mathcal{P}}_{L_x} + \mathcal{C}(k_x^*L_x)\sigma^{2\,\mathcal{P}}_{L_y}, \tag{27}$$

where $\sigma^{2\,\mathcal{P}}$ denotes the SSV for the ocean with the power spectrum $\mathcal{P}$ (formula (17) and the mean value theorem were used here). Dividing by $\langle\mathcal{G}\rangle(L_x^2+L_y^2)/12$, obtain

$$\alpha^{\mathcal{P}}_{L_x\times L_y} = \tilde{\alpha_x} + \mathcal{C}(k_x^*L_x)\tilde{\alpha_y},$$

where

$$\tilde{\alpha}_x = \frac{1}{4}\left[(1+\gamma)(1+\ell)\alpha^{\mathcal{P}}_{L_x}\right], \qquad \tilde{\alpha}_y = \frac{1}{4}\left[(1-\gamma)(1-\ell)\alpha^{\mathcal{P}}_{L_y}\right].$$

Here $\gamma = (\mathcal{G}_x - \mathcal{G}_y)/(\mathcal{G}_x+\mathcal{G}_y)$ measures local anisotropy of variations in the sea surface height and ℓ is the "anisotropy" in the grid, introduced by (22). Since a similar equation can be written for x and y switched, one can write

$$\alpha^{\mathcal{P}}_{L_x\times L_y} = \max(\tilde{\alpha_x},\tilde{\alpha_y}) + \mathcal{C}(\lambda^*_{\max})\min(\tilde{\alpha_x},\tilde{\alpha_y}). \tag{28}$$

With the values of $\mathcal{C}$ being between 0 and 1, equation (28) provides both upper and lower bounds for $\alpha^{\mathcal{P}}_{L_x\times L_y}$.

5 Verification

One-dimensional wavenumber power spectrum. The form of the along-track power spectrum found by S97 involves $k^{-2.5}$ relationship in the tropical oceans and consists of three distinct spectral fragments with exponents -0.7, -2.8, and -4.6 in midlatitudes, the transition points being defined in terms of normalized wavenumbers. For the purposes of the present note, these two spectral forms are joint into a single spectral curve:

$$\Gamma(\tilde{k}) = \begin{cases} A\tilde{k}^{-0.7}, & a_- \le \tilde{k} \le b_- \\ Ab_-^{-0.7-r}\tilde{k}^r, & b_- \le \tilde{k} \le b_+ \\ Ab_-^{-0.7-r}b_+^{r+4.6}\tilde{k}^{-4.6}, & b_+ \le \tilde{k} \le a_+ \end{cases} \tag{29}$$

where $b_- = \max(a_-, 1.006)$, $a_+ = 4.54$, and $\tilde{k} = k/k_0$ is normalized by the wavenumber of maximum kinetic energy k_0. The latter is presented by S97 as a function of the first-mode baroclinic Rossby radius of deformation L_{Ro} and latitude θ:

$$k_0 = [2\pi(0.8+\theta/25^o)L_{Ro}]^{-1}. \tag{30}$$

Poleward of a certain latitude θ_0 parameters in (29) take values determined by S97 for off-tropical spectra: $a_- = 0.18, \quad b_+ = 2.057, \quad r = -2.8$. Equatorward of θ_0, they are interpolated toward their equatorial values (which correspond to a single spectral segment between $a^e_-k_0$ and a_+k_0) by the formulas

$$a_- = 0.18(1-d) + a^e_-d, \quad b_+ = 2.057(1-d) + 4.54d, \quad r = -2.8(1-d) - 2.5d.$$

In order to get a better fit to the observed values, the interpolation coefficient d is chosen to depend on the latitude θ as $d = (\theta_0-\theta)^2/\theta_0^2$, the lower limit for normalized equatorial wavenumbers is

taken a_-^e=1.5, and the "switching" latitude for the equatorial approximation θ_0 is taken θ_0 =30^o when $\Gamma(k_x/k_0)$ approximates $\mathcal{P}_x(k_x)$ and θ_0 =10^o when $\Gamma(k_y/k_0)$ approximates $\mathcal{P}_y(k_y)$. Ratios (26) do not depend on the choice of the constant A. Integrations in (26) are done numerically in the interval of wavenumbers between a_-k_0 and a_+k_0.

One-dimensional averages. Observational ratios

$$\alpha_{L_x} = \frac{12}{L_x^2}\frac{\sigma_{L_x}^2}{\mathcal{G}_x}, \quad \alpha_{L_y} = \frac{12}{L_y^2}\frac{\sigma_{L_y}^2}{\mathcal{G}_y}$$

computed via formulas (1), (3), and (4) from the DLTR data set for $L_x = L_y = 4^o$ are shown in Figure 3 (top panels). They manifest a discernible latitudinal dependence (particularly for α_{L_y}), which underlies more localized features. The dependence on the latitude becomes even more obvious in their zonal means presented in Figure 4 (thick lines) for L_x and L_y taking values 2^o, 4^o, and 8^o. "Unphysical" values of α which exceed 1 due to severe undersampling are excluded from spatial averaging hereafter.

Theoretical values for the same cases are computed via (26) and (29) (Figure 4, dashes). Estimates of L_{Ro} by Chelton et al. (1998) were used in (30) to obtain k_0. The theoretical values are systematically lower than the observational ones, particularly for smaller L_x and L_y. In order to explain the difference, recall that observational values of $\langle\mathcal{G}\rangle$ and $\langle\sigma^2\rangle$ were computed by formulas (1), (3), and (4) which are based on a finite spatial sample or a finite-difference approximation. The theoretical formulas (13) and (14) used in (26) are written for an infinite sample and precise derivatives. Therefore, to achieve better consistency between observational and theoretical estimates, the latter needs to be derived in the way mimicking the treatment of observations. To obtain such a formula for $\sigma_{L_x}^2$ insert $s_n = \exp(i2\pi k_x n\Delta x), n = 1, \ldots, N$ into (4). After some simplifications find

$$\hat{\sigma}_{L_x}^2 = \frac{N}{N-1}\left[1 - \frac{\sin^2\pi k L_x}{N^2\sin^2\pi k\Delta x}\right]. \tag{31}$$

For $\mathcal{G}_x$ use (3):

$$\hat{\mathcal{G}}_x = \left|\frac{e^{i2\pi k_x(m+1)\Delta x} - e^{i2\pi k_x(m-1)\Delta x}}{2\Delta x}\right|^2 = \left(\frac{\sin 2\pi k_x\Delta x}{\Delta x}\right)^2. \tag{32}$$

Estimates (31),(32) and similar ones for the $y-$direction can be used to obtain values

$$\hat{\alpha}_{L_x}^{\mathcal{P}} = \frac{12}{L_x^2}\frac{\int\hat{\sigma}_{L_x}^2\mathcal{P}_x(k_x)dk_x}{\int\hat{\mathcal{G}}_x\mathcal{P}_x(k_x)dk_x}, \qquad \hat{\alpha}_{L_y}^{\mathcal{P}} = \frac{12}{L_y^2}\frac{\int\hat{\sigma}_{L_y}^2\mathcal{P}_y(k_y)dk_y}{\int\hat{\mathcal{G}}_y\mathcal{P}_y(k_y)dk_y}. \tag{33}$$

These show improved consistency with observations (Figure 4, thin solid lines).

Good agreement between observational and theoretical values helps to explain the difference in the latitudinal behavior of α_{L_x} and α_{L_y}. Reduction in the Rossby radius with latitude shifts the power spectra toward shorter waves, which correspond to smaller α ratios. This causes a considerable reduction of α_{L_y} with latitude. In α_{L_x}, on the other hand, the decrease of the Rossby radius with latitude is counterbalanced by the reduction in the length of L_x, in direct proportion to $\cos\theta$. This results in a much weaker dependence of α_{L_x} on latitude.

Two-dimensional averages. Figure 5 compares global means of observational and theoretical values of $\alpha_{L_x\times L_y}$ for various combinations of L_x and L_y. As before, observational values are computed by formulas (1), (3), and (4). One-dimensional theoretical estimates for α_{L_x} and α_{L_y} (corresponding to $L_y = 0$ and $L_x = 0$ respectively, see (25)) are based on (33). The difference

between theoretical and observational values for these estimates correspond to the discrepancies seen in the Figure 4.

Theoretical estimates for $\alpha_{L_x \times L_y}$ corresponding to truly two-dimensional averaging ($L_x > 0$ and $L_y > 0$) are based on the approximation (28). Upper and lower bounds correspond to the values of $\mathcal{C}(\lambda^*_{\max})$ taken equal 1 and 0 respectively ($\lambda^*_{\max}$ at 0 or ∞). Despite the error in theoretical values for α_{L_x} and α_{L_y}, all based on them intervals for $\alpha_{L_x \times L_y}$ indeed contain observational values (Figure 5).

To obtain estimates of $\alpha_{L_x \times L_y}$ value within these intervals, note that the presence of $\mathcal{P}$ in the integral of equation (27) favors the low-wavenumber part of the power spectrum. Therefore $\lambda^*_{\max}$ is taken at the midpoint of the flattest (with the exponent -0.7) portion of the spectrum Γ: $\lambda^*_{\max} = \tilde{k}^* k_0 L_{\max}$ with $\tilde{k}^* = (a_- + b_-)/2$. Near the equator this expression gives the smallest wavenumber in which Γ is defined by (29). Figure 5 demonstrates that this approximation has a reasonable skill.

The theoretical estimates of $\alpha_{L_x \times L_y}$ can be used in formula (12) to compute $\langle \sigma^2_{L_x \times L_y} \rangle$, given $\langle \mathcal{G} \rangle$. The calculated pattern for the case $L_x = L_y = 4^o$ (Figure 1d) is very close to the results of direct computation of $\langle \sigma^2_{L_x \times L_y} \rangle$ (Figure 1a). A comparison of these two patterns on the scatter plot (Figure 2c) shows a very good correspondence indeed, with no apparent latitudinal offsets in the scatter.

6 Discussion and Conclusions

An explicit connection is established between basic statistical and dynamical characteristics of a sea surface field: its small-scale variance in a box of dimensions $L_x \times L_y$ $\langle \sigma^2_{L_x \times L\ _y} \rangle$ and its geostrophic kinetic energy $\langle \mathcal{K} \rangle$ are related by

$$\langle \sigma^2_{L_x \times L_y} \rangle = \alpha_{L_x \times L_y} \frac{2f^2}{g^2} \frac{L_x^2 + L_y^2}{12} \langle \mathcal{K} \rangle$$

(this combines (12) with (2)). The factor $\alpha_{L_x \times L_y}$ is always between 0 and 1 and depends on the two-dimensional wavenumber power spectrum of the sea surface height and dimensions L_x and L_y (see equation (23) and Figure 3).

If the energy distribution over wave directions and the gridbox geometry are fixed, $\alpha_{L_x \times L_y}$ increases with the wavelength (equations (20) and (21)). It tends to zero when waves are very short compared to the grid dimensions and reaches its maximum when the waves are very long. Thus the areas where waves are unusually long have higher values of α. Therefore there is a general increase of α in the equatorial area (Figures 3 and 4) where long equatorial Kelvin and Rossby waves propagate. Also most of the counter current areas and other places with high shear and instability waves are associated with local maxima of α (Figure 3). Another corollary is that the increase in the size of $L_x \times L_y$ grid box causes a decrease in $\alpha_{L_x \times L_y}$. This is clearly confirmed by observations (Figures 4 and 5).

The maximum value which $\alpha_{L_x \times L_y}$ can reach is controlled by the gridbox geometry in relation to the directional distribution of wave energy (equations (20) and (22)). If the distribution is isotropic ($kappa \ll 1$) or the gridbox is square ($\ell = 0$), the maximum value of α is 0.5. In the case of completely anisotropic and perfectly aligned wave and grid geometry $\kappa\ell = 1$, so the maximum is 1 (in practice this corresponds to one-dimensional averaging, when one of the grid dimensions is set to 0). Equation (20) demonstrates this property for individual waves, and Figure 5 shows observations being consistent with it.

Of course, α for the real ocean never reaches its theoretical maximum value (this would require having only infinitely long waves present). Moreover, despite the good agreement between the observational and theoretical values obtained here (Figures 4 and 5), the α values for the real ocean are probably even lower. The reason is that the shortest waves resolved by the satellite altimetry data are of the order of 100km. The agreement between the observational values based on the DLTR data and theoretical values which assume the S97 spectral shape confirms the theory developed here and a consistency between the DLTR and S97 analyses, largely based on the same data (TOPEX altimetry). Still, the presence in the ocean of short waves not resolved by the satellite altimetry makes it plausible that the actual values of α obtained in this note are biased high.

Since the two-dimensional wavenumber spectrum of the sea surface height required by formula (23) is not available at present, the S97 one-dimensional along-track spectrum was used to compute values of α for one-dimensional averaging (equations (33)). Then formula (28) was used to obtain estimates for two-dimensional values of α. Despite a good performance of these one- and two-dimensional estimates (Figure 1a,d, 2c, 4 and 5), they are far from perfect. First, near equator theoretical values deviate from observations even for zonal means (Figure 4), because the wave structure in this area does not obey a simple spectral description (S97). Second, a comparison of observational and theoretical estimates of α for one-dimensional averages (Figure 3) reveals that the latter have a substantially more zonally-uniform structure than the former. Ratios of observed to theoretical values form roughly similar patterns for both α_{L_x} and α_{L_y}. The theoretical error can reach 50% in some locations, although it is below 20% in most places (Figure 3, bottom panels). The error in theoretical estimates for α_{L_x} and α_{L_y} translates into the relative error of a similar pattern and approximately 50% larger amplitude in $\alpha_{L_x \times L_y}$ estimates by (28) (not shown).

Excessively uniform zonal structure is brought into the theoretical estimates of α by the uniform zonal structure of the Rossby radius L_{Ro} on which k_0 depends (see (30)). Observed zonal variations of α are due to the deviations of the real ocean power spectrum from the simplified description (29). Detailed interpretation and better estimates of α will be possible when location-dependent two-dimensional wavenumber power spectra of sea surface height are developed in the future, with further progress in satellite altimetry.

Acknowledgments. The author is greatly indebted to Dr. Mark Cane for his advice on the disposition and content of this note. This research was supported by the NOAA through grants NA86GP0515, UCSIO P.O. 10216264, and NA06GP0567. The hospitality of the Institute for Mathematics and its Applications in University of Minnesota is gratefully acknowledged.

References

Buck, R.C., 1978: *Advanced Calculus*, 3d ed. McGraw-Hill, New York. 622pp.

Chelton, D. B., R. A. deSzoeke, M. G. Schlax, K. El Naggar and N. Siwertz, 1998: Geographical variability of the first-baroclinic Rossby radius of deformation, *J. Phys. Oceanogr.*, **28**, 433-460.

Cheney, R.E., J.G.Marsh, and B.D. Beckley, 1983: Global mesoscale variability from collinear tracks of Seasat altimetry data. *J. Geophys. Res.*, **88**, 4343-4354.

Cheney, R., L. Miller, R. Agreen, N. Doyle, and J. Lillibridge, 1994: TOPEX/POSEIDON: The 2-cm Solution. *J. Geophys. Res.*, **99**, 24,555–24,564.

Ducet, N., P.-Y. Le Traon, and G. Reverdin, 2000: Global high-resolution mapping of ocean circulation from TOPEX/Poseidon and ERS-1 and -2. *J. Geophys. Res.*, **105**, 19,477-19,498.

Fu, L.-L., 1983: On the wave number spectrum of oceanic mesoscale variability observed by the SEASAT altimeter, *J. Geophys. Res.*, **88**, 4331-4341.

Fu, L.-L., D.B.Chelton, and V.Zlotnicki, 1988: Satellite altimetry: observing ocean variability from space. *Oceanography*, **1**(2), 4-11 and 58.

Kaplan, A., M.A. Cane, D. Chen, D. Witter, R. Cheney, 2003: Signal and noise in tropical Pacific sea level height analyses. *J. Geophysical Res.*, in review. [Available from Institute for Mathematics and its Applications, preprint #1903:
`http://www.ima.umn.edu/preprints/dec2002/1903.pdf`].

Kaplan, A., Y. Kushnir, M. Cane, and M. Blumenthal, 1997: Reduced space optimal analysis for historical data sets: 136 years of Atlantic sea surface temperatures, *J. Geophys. Res.*, **102**, 27835–27860.

Leith, C.E, 1973: The standard error of time-average estimates of climatic means. *Journal of Applied Meteorology*, **12**, 1066–1069.

Le Traon, P.Y, M.C. Rouquet, C. Boissier, 1990: Spatial scales of mesoscale variability in the North Atlantic as deduced from Geosat data, *J. Geophys. Res.*, **95**, 20,267-20,285.

Mardia, K.V., J.T. Kent, and J.M. Bibby, 1979: *Multivariate Analysis.* Academic Press, Inc., New York. 521 pp.

Stammer D., 1997: Global characteristics of ocean variability estimated from regional TOPEX/Poseidon altimeter measurements, *J. Phys. Oceanogr.*, **27**, 1743-1769.

Stammer D. and C.Wunsch, 1999: Temporal changes in eddy energy of the oceans, *Deep Sea Res., II*, **46**, 77-108.

Trenberth, K.E., J.R. Christy, J.W. Hurrell, 1992: Monitoring Global Monthly Mean Surface Temperatures. *J. Climate*, **5**, 1405–1423.

List of Figures

(a) Small-scale variability $\langle\sigma^2_{4^o\times 4^o}\rangle$, cm^2 (b) Geostr kinetic energy $\langle\mathcal{K}\rangle$, (cm/s)^2

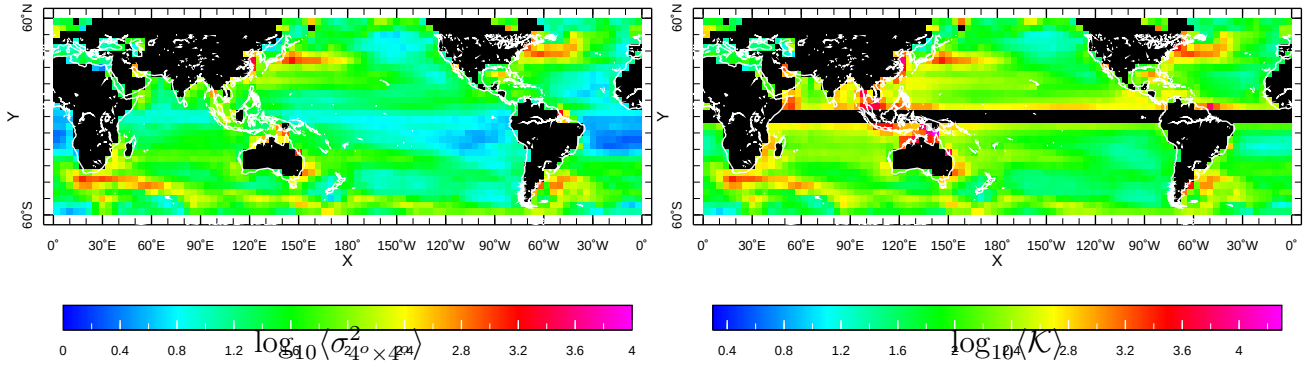

(c) Squared gradient $\langle\mathcal{G}\rangle$ (d) $\langle\mathcal{G}\rangle$-based estimate for $\langle\sigma^2_{4^o\times 4^o}\rangle$, cm^2

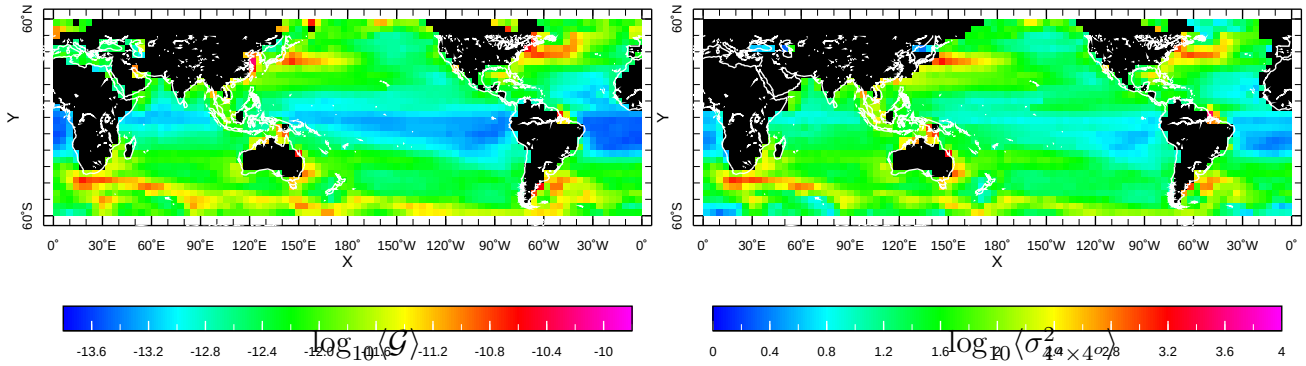

Figure 1: Similarity between SSV and EKG patterns. Shown are base 10 logarithms of numerical values in indicated units of (a) the SSV pattern $\langle\sigma^2_{4^o\times 4^o}\rangle$, cm^2, (b) the GKE pattern $\langle\mathcal{K}\rangle$, (cm/s)^2, (c) the squared gradient $\langle\mathcal{G}\rangle$, dimensionless, and (d) the values of $\langle\sigma^2_{4^o\times 4^o}\rangle$, cm^2, estimated by formula (12). Calculations were done using the DLTR satellite altimetry data set.

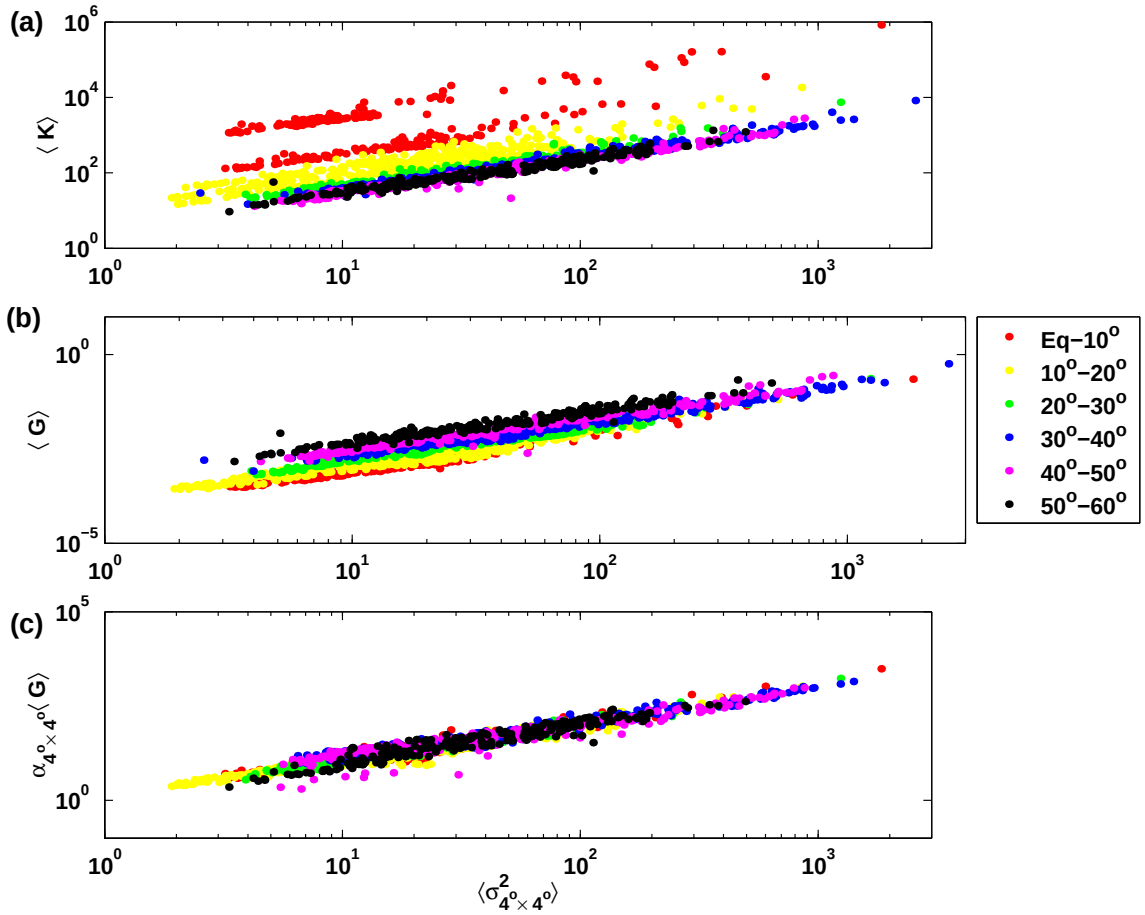

Figure 2: Scatterplots of the small-scale variability $\langle\sigma^2\rangle$ versus (a) the geostrophic kinetic energy $\langle\mathcal{K}\rangle$, (b) squared gradient of sea surface height $\langle\mathcal{G}\rangle$, and (c) $\langle\mathcal{G}\rangle$-based estimate of $\langle\sigma^2\rangle$ by (12). Calculations are done for $4^o\times 4^o$ grid boxes. Colors indicate latitudinal bands.

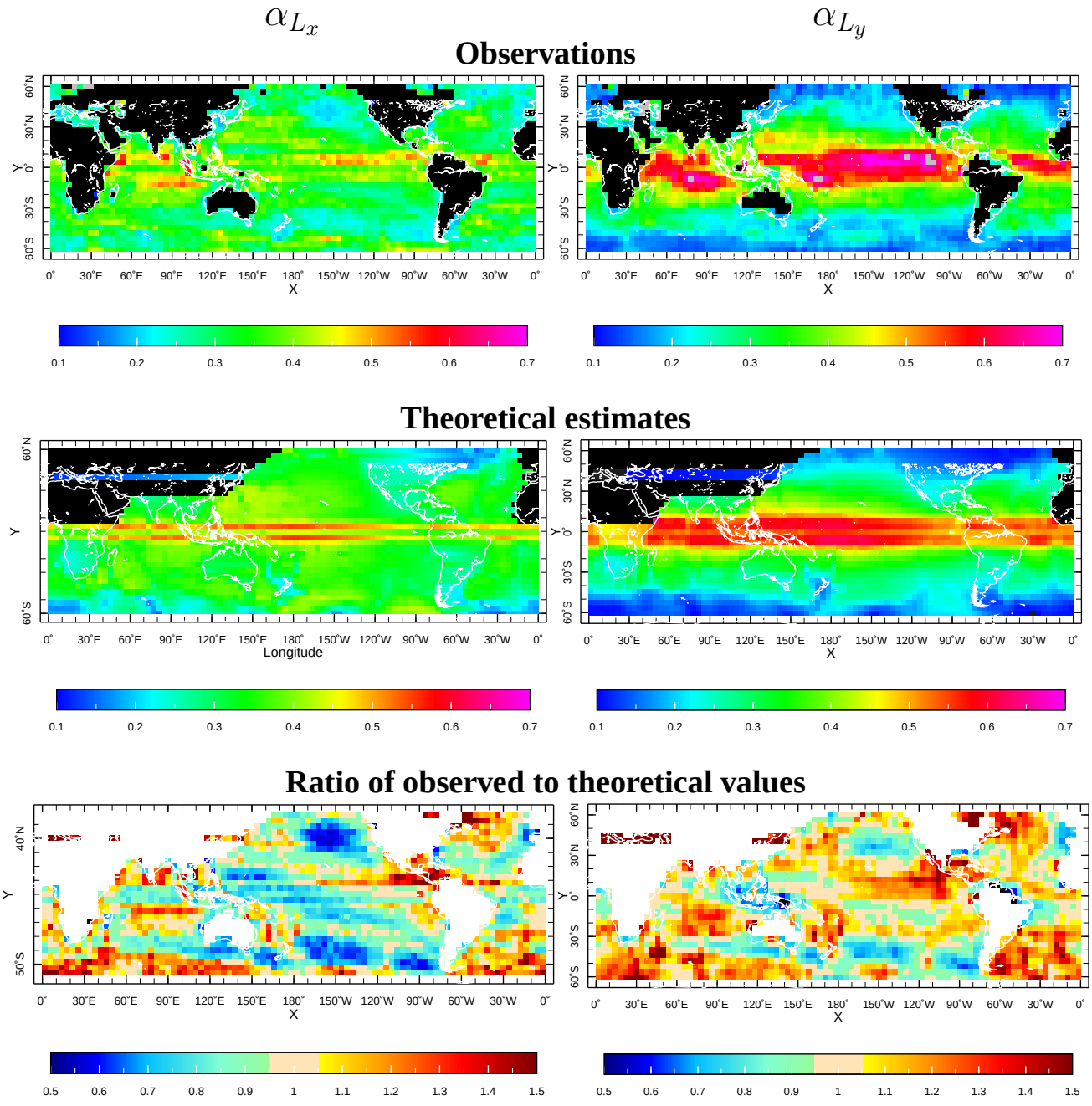

Figure 3: Coefficients (left) α_{L_x} and (right) α_{L_y}: (top) computed from the DLTR data set for $L_x = L_y = 4^o$, (middle) estimated theoretically by formula (33), (bottom) ratio of observed to theoretical values

Zonally averaged values of α for one-dimensional variances

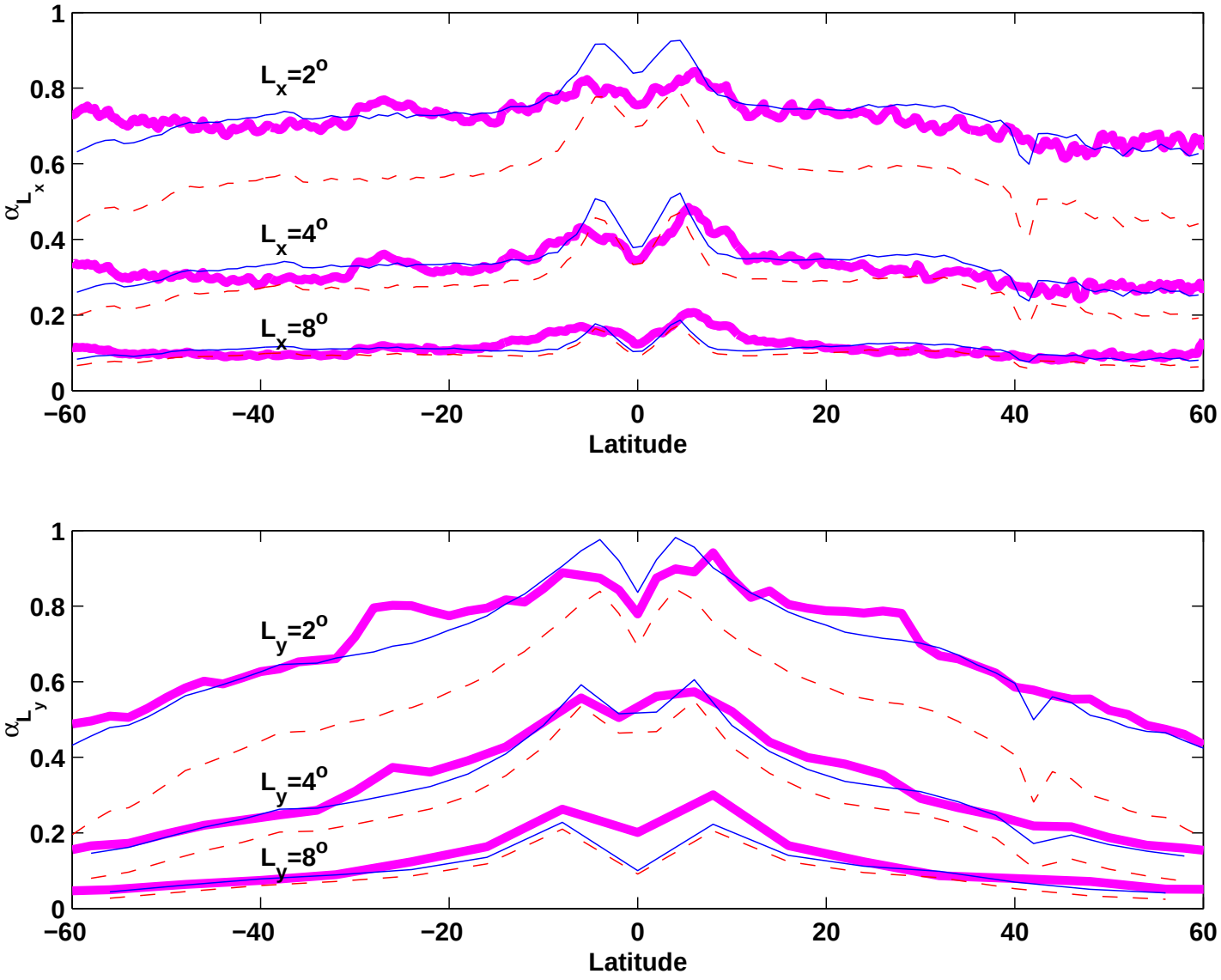

Figure 4: Zonal averages of α_{L_x} (top) and α_{L_y} (bottom) for L_x and L_y equal to 2^o, 4^o, and 8^o. Shown are observed values computed from the DLTR data set (thick lines) and theoretical estimates for continuous (dashed lines) and gridded (thin solid lines) fields, calculated by formulas (26) and (33) respectively .

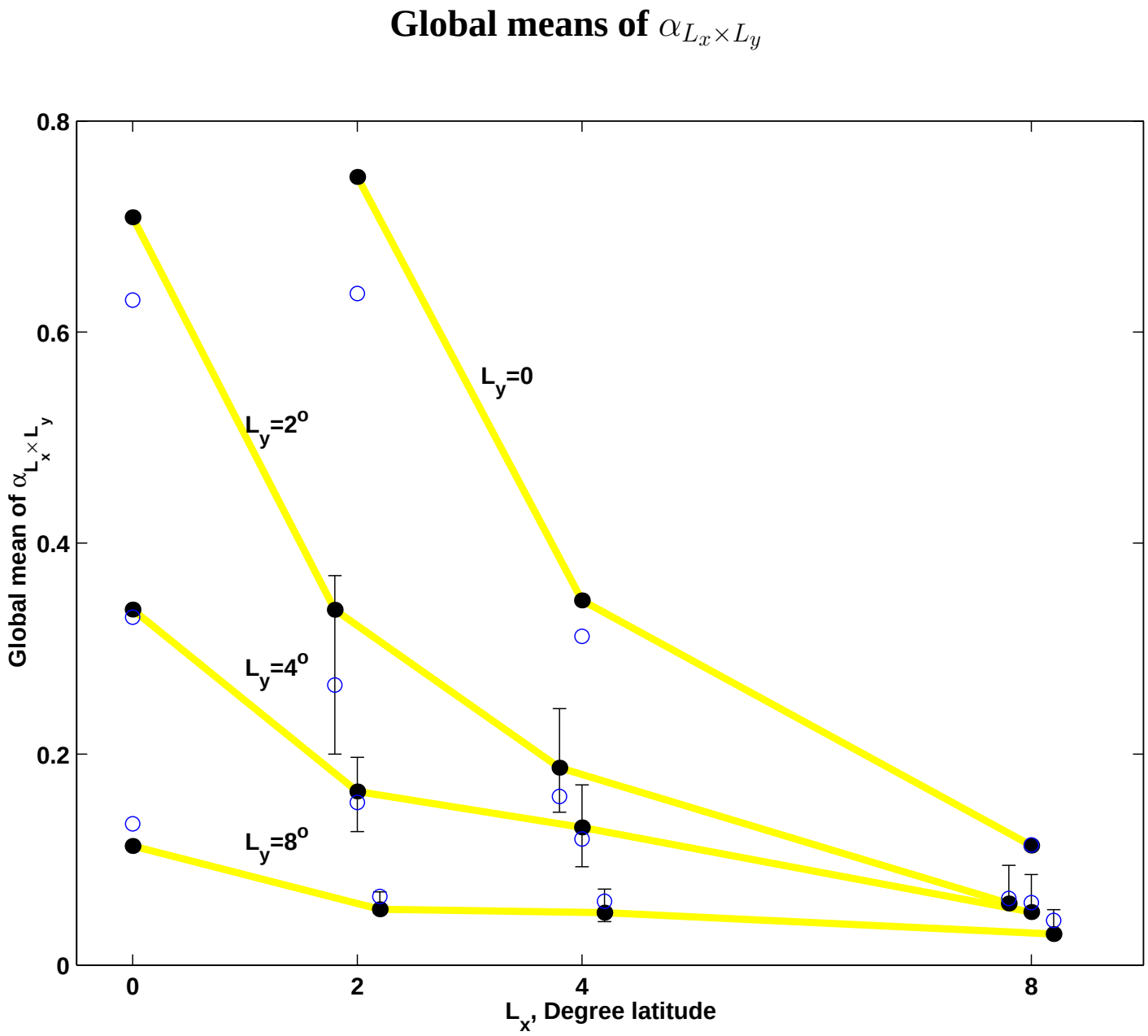

Figure 5: Global means of $\alpha_{L_x \times L_y}$ for L_x and L_y taking values of 2^o, 4^o, and 8^o. Shown are observed values computed from the DLTR data set (empty circles) and theoretical estimates (solid circles) with error bars computed by formula (28). Cases of one dimensional average (L_x or L_y equals to 0) are shown as well. Small horizontal shifts are applied to the circles in order to improve visibility.